ACS APPLIED MATERIALS & INTERFACES

www.acsami.org

Research Article

Hybrid Redox Flow Cells with Enhanced Electrochemical Performance via Binderless and Electrophoretically Deposited Nitrogen-Doped Graphene on Carbon Paper Electrodes

Barun Kumar Chakrabarti,* Jingyu Feng, Evangelos Kalamaras, J. Rubio-Garcia,* Chandramohan George, Hui Luo, Yuhua Xia, Vladimir Yufit, Maria-Magdalena Titirici, Chee Tong John Low, Anthony Kucernak, and Nigel P. Brandon

Cite This: *ACS Appl. Mater. Interfaces* 2020, 12, 53869–53878

Read Online

ACCESS | Metrics & More | Article Recommendations | Supporting Information

ABSTRACT: Hybrid redox flow cells (HRFC) are key enablers for the development of reliable large-scale energy storage systems; however, their high cost, limited cycle performance, and incompatibilities associated with the commonly used carbon-based electrodes undermine HRFC's commercial viability. While this is often linked to lack of suitable electrocatalytic materials capable of coping with HRFC electrode processes, the combinatory use of nanocarbon additives and carbon paper electrodes holds new promise. Here, by coupling electrophoretically deposited nitrogen-doped graphene (N-G) with carbon electrodes, their surprisingly beneficial effects on three types of HRFCs, namely, hydrogen/vanadium (RHVFC), hydrogen/manganese (RHMnFC), and polysulfide/air (S-Air), are revealed. RHVFCs offer efficiencies over 70% at a current density of 150 mA cm^{-2} and an energy density of 45 Wh L^{-1} at 50 mA cm^{-2}, while RHMnFCs achieve a 30% increase in energy efficiency (at 100 mA cm^{-2}). The S-Air cell records an exchange current density of 4.4×10^{-2} mA cm^{-2}, a 3-fold improvement of kinetics compared to the bare carbon paper electrode. We also present cost of storage at system level compared to the standard all-vanadium redox flow batteries. These figures-of-merit can incentivize the design, optimization, and adoption of high-performance HRFCs for successful grid-scale or renewable energy storage market penetration.

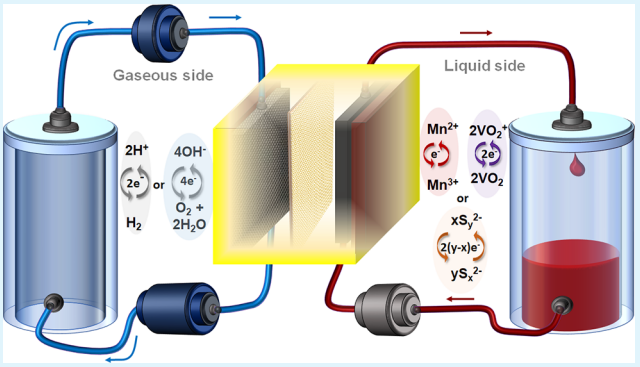

KEYWORDS: *hybrid redox flow cell, hydrogen, vanadium, nitrogen-doped carbon, grid-scale energy storage*

1. INTRODUCTION

Developing large-scale electrochemical energy storage technologies without compromising energy efficiency, power density, safety, and cost-effectiveness is one of the biggest challenges in enabling the transition into renewable energies, especially via grid-scale storage and back-up power storage for intermittent energy sources.[1,2] Redox flow batteries (RFBs) have been extensively investigated since the 1960s for large-scale stationary energy storage because their engineering flexibility can be better than alternatives such as pumped hydro or compressed air systems.[3] RFBs promise a long cycle life, decoupled power and energy characteristics, and round-trip energy efficiencies as high as 85% (normally operating below a current density of ~120 mA cm^{-2}), but their commercial exploitation has been limited by high capital costs due to the use of expensive vanadium-based electrolytes (about ~43% of system cost for a 4 MWh all-vanadium RFB)[4] and membranes. As most of electrode designs are not yet optimized, they are not suitable for flow battery operation at high current densities. For the cost reduction of RFBs several strategies have been undertaken, for example, adopting low-cost electrolytes such as for polysulfide/bromine RFBs,[5] aqueous−organic systems,[6] redox-mediated RFBs,[7] and hydrogen/bromine (RHBrFC),[8] hydrogen/benzoquinone,[9] and polysulfide/air (S-Air)[3] hybrids. The latter three are known as gas/liquid hybrid redox flow cells (HRFC). Despite the advantage of using abundant chemicals (e.g., sulfur, bromine, air, and/or hydrogen), the tendency of bromine to form toxic vapors as well as poisoning and/or corroding the HOR/HER (hydrogen oxidation reaction/hydrogen evolution reaction) catalyst materials still limits the widespread use of RHBrFCs.[10] Surprisingly, a vast majority of HRFC studies have focused on improving peak power densities (see Table S1 in the

Received: September 30, 2020
Accepted: October 27, 2020
Published: November 18, 2020

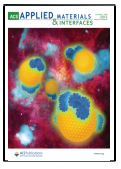

Supporting Information exemplifying historical developments in HRFCs since the 1960s), which is not a representative indicator of the actual performance of both HRFCs and RFBs because at high power conditions, electrolyte utilization is normally poor.[9,11] For cost-effectiveness and maximizing the benefits of RFBs and HRFCs, they need to be operated at higher current densities, as this can effectively reduce the size and number of cells per stack (thereby their costs). This basically depends on how efficiently HRFC electrodes are engineered in terms of their microstructural features and the extent to which they can cope with their harsh operating conditions.[12] Practically, HRFC electrode performances are dictated by electrode microstructure and surface chemistry setting the actual operational parameters, which are in turn influenced by the following properties: (i) wettability of electrodes, (ii) pressure drop affecting mass transport, (iii) electrochemical surface area (ECSA), (iv) charge transport, and (v) electrical conductivity and mechanical stability under a given cell compression.[13−15] Most commonly, carbon-based materials are used as electrodes for RFBs, particularly in the commercially exploited all-vanadium RFB (VRFB),[16] where carbon-based electrodes are subject to thermal or chemical processes for activation as a means to improve the electrochemical performance of VRFB electrodes[17] (as detailed in Table S2). The key performance indicators evaluated for these electrodes with respect to activation processes involve round-trip efficiency and capacity utilization at increasing operational current density. The use of carbon-based electrodes is preferred for VRFBs because they are less prone to corrosion even in highly acidic environments of 3−5 M sulfuric acid[2] and are most cost-effective. Similarly, studies have reported that performance improvements are due to higher ECSA and wettability as a consequence of electrode surface modifications by carbon nanostructures that have catalytic activities, which include carbon nanotubes (CNTs), graphene (G), and nitrogen-doped graphene (N-G).[18] Such strategies have been in part extended to HRFCs; for example, Tenny et al.[19] reported the use of multiwall CNT-modified cloth in the regenerative hydrogen/vanadium fuel cell (RHVFC), evidencing improvements on power density. Similarly, reduced graphene oxide (rGO)-modified commercial carbon as electrodes in the RHVFC were shown to yield a 10% improvement in terms of energy efficiency and electrolyte utilization for up to 10 charge and discharge cycles.[12]

On the other hand, replacing vanadium-based electrolytes with more abundant manganese led to the introduction of a low-cost RFC (RHMnFC),[20] which displayed higher peak power densities as well as energy efficiencies when using carbon felts in comparison to carbon paper (CP). Despite good electrode stability (in 3 M sulfuric acid at a cell potential of 1.5 V), carbon felts are thicker than carbon papers and require higher pumping power to achieve similar flow velocity as CP electrodes in RFBs, thus potentially offsetting their cost-effectiveness.[21] Another potential low-cost and inherently safe-to-operate HRFC (due to the use of nonvolatile materials compared to RHBrFC) is the aqueous-based S-Air, proposed by Brandon et al.[22] which is still in its very early stage of development.[3] Clearly, advanced HRFC application requires a systematic understanding of how chemical, catalytic, defects, and surface properties enabled by electrode modification that had positively impacted RFBs would translate into the levels of electrode specificity required for HRFCs' electrochemistry and how they cope with their harsh operating conditions. Additionally, in contrast to the highly acidic medium of RHVFC and RHMnFC, S-Air cells operate under highly corrosive but alkaline conditions, requiring electrode surfaces with good catalytic activity,[3] and S-Air chemistries greatly suffer from the irreversibility of polysulfides. As such, there is still a lack of understanding as to how HRFC reactions are practically mediated by carbon-based electrodes that are modified with controlled deposition of oxygen- or nitrogen-rich additives. Therefore, here we propose a simple electrode design involving modification of standard carbon paper electrodes (CP) with electrophoretically deposited N-G and demonstrate their suitability for three types of HRFCs such as RHVFC, RHMnFC, and S-Air (as illustrated in Scheme 1) by

Scheme 1. A Binder-Free Horizontal Electrophoretic Deposition (EPD) Process Is Used to Activate Commercial Carbon Paper Electrodes Using Nitrogen-Doped Graphene[a]

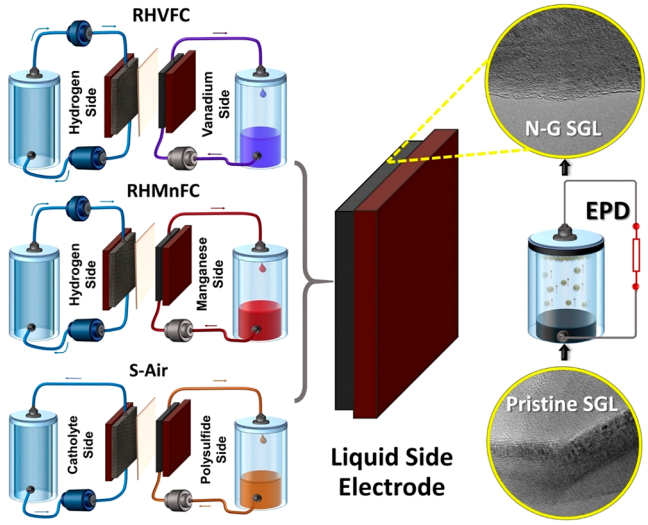

[a]These modified electrodes are employed in three types of hybrid redox flow cells (HRFC), namely hydrogen/vanadium (RHVFC), hydrogen/manganese (RHMnFC), and polysulfide/air (S-Air). A typical HRFC consists of an electrochemical cell, storage tank, and hydrogen or oxygen gas cylinder. The anolyte and catholyte are separated by a nafion proton-exchange membrane (in the S-Air cell, the membrane used is similar to sodium ion exchange), respectively.

revealing the beneficial effects on vanadium (VO^{2+}/VO_2^+), manganese (Mn^{2+}/Mn^{3+}), and polysulfide chemistries (S_2^{2-}/S_4^{2-}), resulting in good performance of HRFCs. The enhancements achieved together with the projected cost-of-storage compared to standard VRFBs (commercial) further highlight their commercial applicability.

In a typical RHVFC, during charging the energy is stored in the form of hydrogen and vanadium(V) (VO_2^+) (eq 1), and during discharge, hydrogen is consumed at the negative electrode and VO_2^+ is reduced to vanadium(IV) (VO^{2+}) at the positive electrode (eq 1).[12] In the RHMnFC, the $Mn^{2+/3+}$ redox couple enables charge/discharge cycles as shown in eq 2.[20] In an S-Air hybrid flow cell, the aqueous polysulfide anolyte is pumped through a porous media at the anode compartment where redox reactions of soluble polysulfide/sulfur take place. Concurrently, the ORR/OER (oxygen reduction reaction/oxygen evolution reaction)[23] takes place at catalytically active gas diffusion media at the cathode

https://dx.doi.org/10.1021/acsami.0c17616
ACS Appl. Mater. Interfaces 2020, 12, 53869−53878

compartment according to the simplified electrode reactions in eq 3.[3]

$$2VO_2^+ + 2H_3O^+ + H_2 \leftrightarrow 2VO^{2+} + 4H_2O \quad E^0_{cell} = 0.99\ V \tag{1}$$

$$Mn^{2+} + 2H^+ \rightarrow Mn^{3+} + H_2 \quad E^0_{cell} = 1.51\ V \tag{2}$$

$$xS_y^{2-} + 4OH^- \leftrightarrow yS_x^{2-} + O_2 + 2H_2O \quad E^0_{cell} = 0.85\ V \tag{3}$$

2. EXPERIMENTAL SECTION

2.1. Materials. Vanadium(IV) oxide sulfate (hydrated) was purchased from Sigma-Aldrich (purity >99%). Manganese carbonate, titanium oxysulfate, Na_2S_2, and NaOH were also obtained at 99% purity from Sigma-Aldrich. Sulfuric acid (5 M) was obtained from Fluka, and *N,N′*-dimethylformamide (DMF, Technical grade for electrophoretic deposition, 94% pure) was purchased from VWR International. Reduced graphene oxide (rGO) was purchased from ACS Material (USA), and all chemicals were used as received. Few-layer graphene was supplied by our collaborators from Manchester University.

2.2. Nitrogen Doping of Graphene. N-G was prepared via a one-pot hydrothermal reaction by using graphene as the carbon source and cyanamide (Merck) as the nitrogen precursor, followed by freeze-drying with a high-temperature calcination as reported in detail elsewhere.[23]

2.3. Cell Assembly and Conditioning. The vanadium-side carbon paper (SGL 10AA gas diffusion layer, 400 μm thick) for the RHVFC was purchased from SGL Carbon Ltd., and the hydrogen-side platinized carbon paper electrode (SGL 29BC, 235 μm thick, 0.3 mg cm^{-2} Pt loading) was obtained from Fuel Cell Store. A well-hydrated Nafion 115 membrane (127 μm thick, Fuel Cell Store) was sandwiched between both electrodes to prepare the membrane electrode assembly (MEA). The membrane was hydrated by heating it in 1 M H_2SO_4 solution for 1 h at 80 °C and then washed with deionized water. In addition, for RHVFC experiments, the hydrogen gas was flowed through a deionized water reservoir to allow humidification of the MEA, which was not necessary for the RHMnFC. After the flow cell was assembled, electrolyte was allowed to run through the system at zero load for at least 1 h while hydrogen gas was sparged through a glass vessel filled with water to ensure the membrane was exposed to moisture from both half-cells.[12]

The humidified hydrogen (CP grade, BOC) was passed through the anodic side at a constant flow rate of 100 mL min^{-1} for polarization experiments or 30 mL min^{-1} for charge and discharge, while a glass reservoir was connected to the hydrogen outlet to collect any vanadium electrolyte crossover.[12] All experiments were conducted at room temperature and pressure. For RHMnFC experiments, the hydrogen was not humidified and Mn crossover was not observed.

For the S-Air system, a homemade 5 cm^2 flow cell assembly was used. The negative electrode (air side) was a 0.9 mm thick sulfidized Ni foam (Goodfellow), whereas the positive electrode was either SGL 10AA or its modified versions. The Ni foam was sulfidized by impregnating it in 1 mol kg^{-1} Na_2S_2/1 mol kg^{-1} NaOH solution for 72 h. Nafion 117 was used as the membrane (also purchased from Fuel Cell Store). The as-received Nafion 117 membrane is in the hydrogen ionic (H^+) form. However, the S-Air RFB system requires a membrane with the sodium ionic (Na^+) form. To exchange the H^+ ions with Na^+ ions, the Nafion membrane needs to be impregnated in 1 mol kg^{-1} NaOH solution for at least 4 h at 18−30 °C.

2.4. Electrolyte Preparation and Circulation. For RHVFC experiments, vanadium sulfate electrolyte solutions were prepared at a concentration of 0.8 M dissolved in 5 M sulfuric acid based on previously utilized electrolytes for VRFBs, some of which provided high power densities (in excess of 1 W cm^{-2}).[11,24] The volume of electrolyte used was 60 mL. For RHMnFC experiments, 1 M manganese carbonate (99.99%, Sigma-Aldrich) solution in a 1 M titanium oxysulfate (Fisher Scientific) electrolyte dissolved in 4 M sulfuric acid was prepared as reported in the literature.[20] A peristaltic pump (Cole-Parmer Masterflex Model 77200-50) was used to circulate the vanadium or manganese electrolyte between the cell and the reservoir at a constant flow rate of 50 mL min^{-1}.

A 1 M polysulfide solution was also prepared for linear sweep voltammetry analyses using sodium sulfide (electrochemically active species, Merck) and sodium hydroxide (Fisher Scientific) as supporting electrolyte. For flow cell polarization experiments, polysulfide electrolyte was circulated between the anode and the anolyte reservoir by using a Cole-Parmer Masterflex peristaltic pump at 50 mL min^{-1}. The catholyte (air) was pumped by a Waston-Marlow 505 U permeate pump at 100 mL min^{-1}. A PTFE filter was attached to the air inlet to remove the impurities (i.e., dust) from the air before being pumped into the cathode compartment.

2.5. Electrophoretic Deposition (EPD). A horizontal EPD reactor was used to deposit 0.1 g L^{-1} of rGO (dispersed in DMF) on CP samples for 30 min at 300 V (TTI Inc. provided the power supply). This procedure was similar to that described in our earlier work.[12,25] Deposits were performed on one side of the carbon paper sample only as double-sided deposits resulted in poor performances.[25] Only the vanadium- or manganese-side electrode (positive electrode) was modified, namely, (1) SGL-pristine SGL 10AA carbon paper electrode, (2) rGO/SGL-carbon paper modified with rGO, and (3) N-G/SGL - carbon paper modified with N-G. For all cases, the rGO and N-G deposits faced the membrane for better electrochemical performances (minimization of ohmic losses) as guided by results we obtained from our previous studies on the RHVFC.[12] The deposition parameters of the horizontal reactor were verified by using a standard vertical EPD reactor using Al foil or Ni foam working electrodes (WEs) and a platinized titanium mesh as the counter (electrodes were obtained from Goodfellow). After this, rGO or N-G was deposited onto carbon papers by using different voltages, times, active material concentrations, dispersion timing (Fisherbrand ultrasound was used to disperse the rGO or N-G in DMF for at least 1 h prior to EPD), and stirring rates and compared with the results obtained from horizontal depositions.

2.6. RHVFC Experiments. The galvanostatic tests were performed by using a Bio-Logic potentiostat (VSP-300), and data logging was performed by using EC-Lab software. For all tests, the RHVFC system was allowed to reach an upper cutoff voltage of 1.4 V and a lower cutoff voltage of 0.4 V as in the previous investigations.[26] This was done to ensure high electrolyte utilization and also to minimize side reactions such as OER. We used 0.8 M $VOSO_4$ in 5 M H_2SO_4 as the positive electrolyte with a total volume of 60 mL and a flow rate of 50 mL min^{-1}.

Electrochemical impedance spectroscopy (EIS) was performed under OCP conditions with a state-of-charge (SOC) of 100%. The EIS measurements were performed after the first galvanostatic charge of fresh solution of vanadium electrolyte at a current density of 10 mA cm^{-2}. EIS was recorded at open-circuit voltage for all samples tested. These measurements were run with an AC current root-mean-square value of 0.005 A over a frequency range from 1 MHz to 100 mHz and with 6 points per decade of frequency. The SOC of the cell was calculated by comparing the experimental capacity with the maximum theoretical capacity (100% SOC).

Single-cycle charge−discharge tests were performed at constant current densities in the range 50−200 mA cm^{-2} for the RHVFC. Finally, potential−current density characteristic curves were obtained at an initial SOC of 100%, by applying steps of galvanostatic discharge at constant current densities in the range 40−500 mA cm^{-2} (30 s discharge followed by 120 s rest between each discharge step), similar to that reported in the literature.[12,26] However, as this was not a single-pass system, it is highly likely that our system experienced electrolyte depletion during measurements, which resulted in lower power output than what was reported previously.[19] 150 charge and discharge tests were performed at 100 mA cm^{-2} to determine the cycling effects on electrodes.

2.7. RHMnFC Experiments. For RHMnFC experiments the cutoff voltages were 1.65 V (upper) and 0.6 V (lower) to minimize MnO_2 precipitation which would occur as a result of a two-electron oxidation.[20] Therefore, the upper cutoff voltage was kept above the

https://dx.doi.org/10.1021/acsami.0c17616
ACS Appl. Mater. Interfaces 2020, 12, 53869−53878

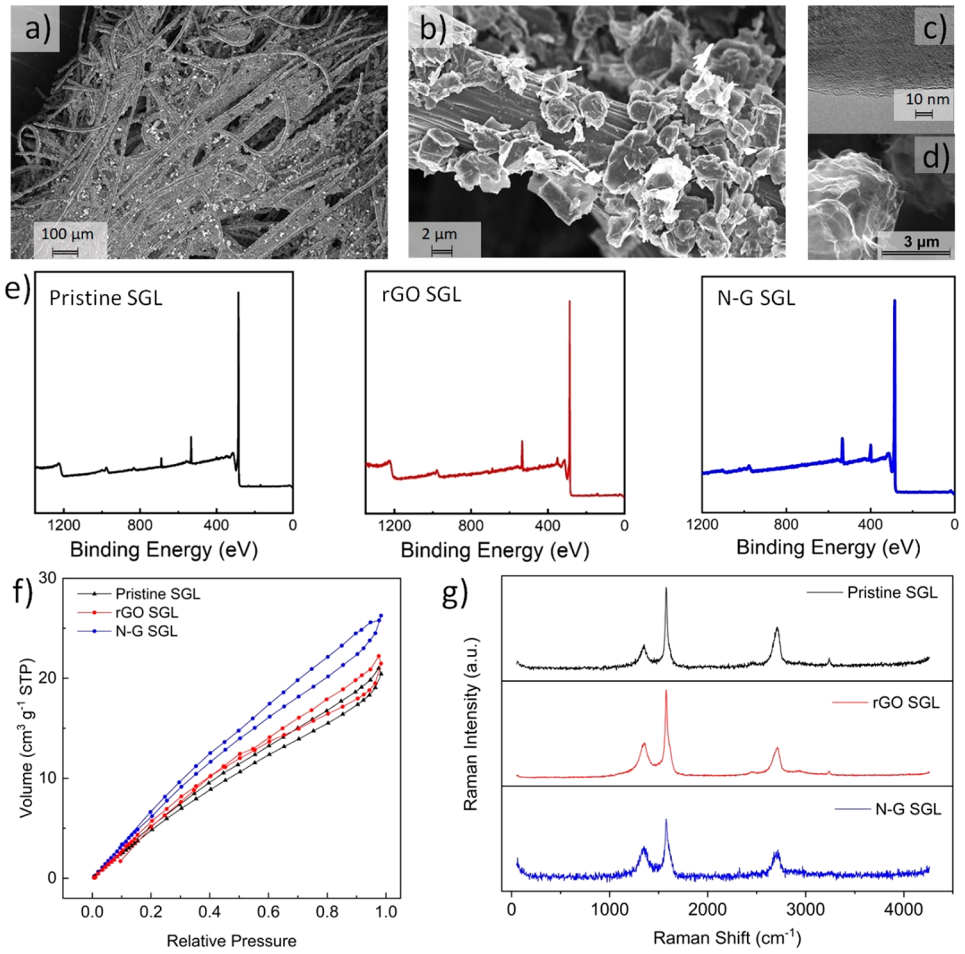

Figure 1. (a) Low-resolution SEM of nitrogen (N)-doped graphene (N-G) deposited on SGL (N-G SGL). (b) SEM of N-G SGL showing CP fiber node covered with N-G flakes. (c) Magnified view of N-G SGL showing transparent nature of the deposited graphene. (d) High-resolution TEM image of N-G SGL. (e) XPS spectra of pristine CP (SGL), reduced graphene oxide (rGO)-modified CP, and N-G-modified CP as electrode materials. (f) BET isotherms of pristine CP, rGO/CP, and N-G/CP electrodes. (g) Raman images of all the CPs applied as electrodes in RHVFCs. I_D/I_G(SGL) = 0.2, I_D/I_G(rGO SGL) = 0.4, and I_D/I_G(N-G SGL) = 0.7.

open-circuit cell voltage of 1.5 V. Charge/discharge experiments were otherwise similar to that for the RHVFC. Charge and discharge cycling was performed at 100 mA cm^{-2} to a maximum of 50 times.

2.8. Linear Sweep Voltammetry of Polysulfide Half-Cell Electrolyte. Linear sweep voltammetry (LSV) of polysulfides in alkaline electrolyte, corresponding to the case of the polysulfide/air flow system, employed a three-electrode cell that consisted of a carbon paper working electrode, a platinum counter electrode, and a saturated Ag/AgCl reference electrode with salt bridge (Metrohm). The working electrolyte used 100 mL of a 1 mol kg^{-1} Na_2S_2 and 1 mol kg^{-1} NaOH solution. Polarization tests of the pristine and modified SGL 10AA electrodes were conducted by using the LSV method and performed between the overpotential window of ±200 mV with a scan rate of 1 mV s^{-1}. Experiments were performed at 20 ± 3 °C, and electrolytes were kept under a nitrogen atmosphere throughout the experiments.

2.9. S-Air Flow Cell Polarization. The single-cell S-Air RFB system was allowed to run without load for a period of time (i.e., 30 min) after setup to reach a stable OCV. The charge cutoff voltage was set to 0.85 V. The polarization curve of the S-Air RFB was obtained by using a chronopotentiometry method. A constant current was applied to the RFB for a certain period of time (i.e., 60 s) where the corresponding steady-state cell voltage was recorded as a data point for the polarization curve, after which the RFB was allowed to rest at its OCV for a period of time (i.e., 2 min) to reach the steady state before the next polarization step.

2.10. Cyclic Voltammetry to Determine Electrochemical Surface Area. Electrochemical measurements were performed by using a Multichannel AUTOLAB M101. The electrode samples (i.e., SGL, rGO/SGL, and N-G/SGL) were used as the working electrode, connected to a platinum plate as current collector. A conventional three-electrode cell was employed, incorporating SCE as the reference electrode and a Pt rod as the counter electrode, and the working electrode was soaked in the electrolyte for 9 h prior to measurements. The electrolyte was 5 M H_2SO_4 solution. All experiments were performed at 20 °C, and electrolytes were sparged with nitrogen for at least 10 min before commencing CV for deaeration purposes. CV experiments were performed between −0.4 and 1.2 V at several scan rates ranging from 2 to 50 mV s^{-1}, similar to that reported previously.[25]

2.11. Morphological Characterization. Scanning electron microscopy (SEM) was performed on a Zeiss Leo Gemini 1525. High-resolution transmission electron microscopy (HRTEM) imaging was performed by using a FEI TITAN 80/300 TEM instrument operating at a voltage of 300 kV. Raman spectra were obtained by using a Senterra II spectrometer. The source of radiation was a laser with a wavelength of 514 nm. Calculation of the parameters I_D/I_G (integrated intensity ratio) and FWHM of the G band was performed by the deconvolution of the spectra. The curve fitting was performed with the combination of Gaussian−Lorentzian line shapes. X-ray photoelectron spectroscopy (XPS) was conducted on a Thermo Scientific Nexsa XPS system employing a monochromatic Al Kα X-ray source.

https://dx.doi.org/10.1021/acsami.0c17616
ACS Appl. Mater. Interfaces 2020, 12, 53869−53878

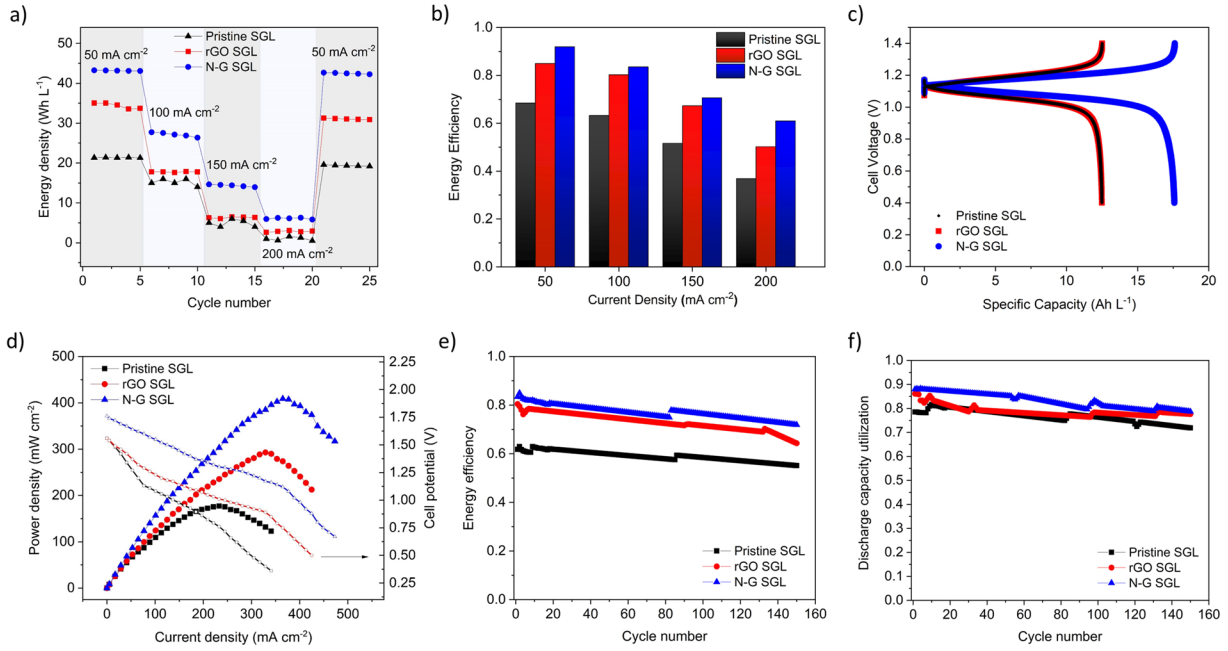

Figure 2. Electrochemical performance of RHVFC using N-G/SGL, rGO/SGL, and pristine SGL as electrodes: (a) Energy density at varying current densities as a function of cycle number. (b) Energy efficiencies as a function of operating current densities. (c) Fifth charge and discharge capacity of RHVFC. Electrolyte was 0.8 M $VOSO_4$ in 5 M H_2SO_4 at a flow rate of 50 mL min^{-1} in a 5 cm^2 active reactor. Hydrogen flow rate was 30 mL min^{-1}, and a constant charge/discharge current density of 50 mA cm^{-2} was used. (d) Polarization and power density curves using the same electrolytic conditions with the exception of a higher hydrogen flow rate of 100 mL min^{-1}. (e) Energy efficiency variation as a function of cycle number under same electrolytic conditions and gaseous flow rate of 30 mL min^{-1}. (f) Discharge capacity utilization for 150 cycles. For both plots (e) and (f) the current density applied was 100 mA cm^{-2}.

Nitrogen sorption isotherms were performed at −196 °C in an IQ3 Quantachrome system. The BET surface area was deduced from an analysis of the isotherm in the relative pressure range of 0.07−0.25 atm. The total pore volume was calculated from the amount of nitrogen adsorbed at a relative pressure of 0.90 atm. The pore size distribution was calculated by the QSDFT method using the adsorption part of the isothermal data.

3. RESULTS AND DISCUSSION

Carbon paper (CP) acting as a gas diffusion layer (SGL 10AA, henceforth termed SGL) was used as the positive electrode for both the RHVFC and RHMnFC and as the negative electrode for S-Air cells (the latter was in a three-electrode system to evaluate the effect of N-G modification of CP in alkaline polysulfide reactions), as shown in Scheme 1. To modify the SGL with either rGO or N-G, a horizontal electrophoretic deposition (EPD) process was used (a binderless process with precise control of few-layer graphene particles deposition with the exclusion of graphene aggregates).[12,25] Deposition methods using the horizontal EPD reactor are detailed in the Experimental Section and also reported elsewhere.[12,25] In Figure 1a, the SEM image shows an SGL (CP) electrode with electrophoretically deposited N-G. The SEM images of pristine SGL and rGO/SGL are supplied in the Supporting Information (Figures S1 and S2). N-G flakes in aggregates can be seen attached to carbon fibers of SGL CP (termed SGL in Figures 1a−c) despite not using a binder. SEM and TEM images of N-G used for the deposition are shown in Figure 1c,d (with detailed images of pristine and cycled electrodes provided in the Supporting Information). The estimated flake density of N-G samples was found to surpass that of rGO and pristine SGL samples (Table S3). A higher density of N-doped carbon materials was reported to provide a greater number of active sites for the adsorption of vanadium ions and their catalytic oxidation in VRFBs.[27] From the SEM images, it was deduced that N-G-modified SGL (N-G/SGL) contained ∼40% more conductive graphitic structures than pristine SGL (Figure 1a−d). The mass loading of N-G was ∼0.25 mg cm^{-2} while it was 0.15 mg cm^{-2} in the case of rGO-modified SGL (rGO/SGL) (Table S3).

Although XPS data of rGO/SGL and pristine SGL look identical, the presence of nitrogen (N) was well evident from the peaks close to 300, 400, and 530 eV in the case of N-G/SGL (as shown in Figure 1e and a closer analysis of the peaks is presented in Figure S11). Because of sp^3-hybridized molecular orbitals of N forming compounds involving three bonds, they leave behind a lone pair of electrons that may hop to the adjacent carbon atoms; therefore, N-doping results in improved electronic conductivity of electrodes.[27] In addition, N-doping better facilitates the interaction between water molecules and doped carbon (related to wettability). More detailed XPS results with N as dopants is given in the Supporting Information. Briefly, four types of N species are observed in N-G/SGL electrodes—pyridinic N (48%), quaternary/graphitic N (24%), pyrrolic N (20%), and oxidized N (8%)—and these N species appear to be distributed as surface functional groups on graphene layers as well as dopants into the interiors of graphene particles (see Figure S11). Among these species quaternary nitrogen is considered to be catalytically active toward VO_2^+/VO^{2+} redox reactions.[18]

BET data as in Figure 1f indicate that N-G/SGL electrodes have a surface area of 45.8 m^2 g^{-1} compared to rGO ∼ 41 m^2 g^{-1} and CP ∼ 30 m^2 g^{-1}. These data are supported by ECSA of electrodes that were estimated from surface capacitance data obtained via cyclic voltammetry and were found to be about 2 orders of magnitude less than BET areas for SGL and rGO/

https://dx.doi.org/10.1021/acsami.0c17616
ACS Appl. Mater. Interfaces 2020, 12, 53869−53878

SGL. In contrast, the ECSA of N-G was only 1 order of magnitude below that of the corresponding BET area (Table S3). The ECSA depends on factors such as the surface wettability and extent of microporous network within electrodes, and a lower value of ECSA can be an indicator for issues such as inaccessible pore network and tortuosity impeding redox/active species adsorption/diffusion.[13] Therefore, the higher surface area combined with larger pore network as observed in N-G/SGL should favor better HRFC kinetics.

Figure 1g shows the Raman spectra obtained on N-G/SGL, rGO/SGL, and pristine SGL electrodes. The intensity of the D peak is low for pristine SGL, indicating the presence of many graphitic layers. In the case of rGO/SGL, the intensity of the D peak becomes relatively higher, which indicates the presence of few or multilayered graphene particles attached to SGL.[21] In the case of N-G/SGL, the D peak intensity is slightly larger in comparison to rGO, which is indicative of a more amorphous nature of the carbon deposits. As such, the 2D peak of rGO/SGL is similar to pristine SGL but slightly less intense compared with N-G/SGL electrodes. Higher D/G ratios are indicative of highly defective crystal structures, and the ratios decrease as the carbon becomes more graphitic (especially for the case of pristine SGL). In brief, these characterizations indicate that the integration of N-G into SGL should in principle render them more suitable as electrodes for HRFCs because of (i) more active sites via enhanced surface area, (ii) resilience against corrosion via robust functional groups, and (iii) higher catalytic activities due to increased defects.[27]

After conducting morphological analyses of the CP samples, we tested them in three different HRFC systems. First, we conducted extensive tests on RHVFCs using the three types of electrodes (as described above) to benchmark their electrochemical performance against that of commercially available liquid−liquid all-vanadium RFBs (standard). We then tested these electrodes on RHMnFCs which require chemically very stable electrodes at high voltages and evaluated their electrochemical performance and corrosion resistance. On the basis of the above tests, we investigated how these electrodes can be further utilized in S-Air HRFCs (as positive electrodes) which typically show sluggish kinetics and operate in alkaline electrolytes. For this, a three-electrode configuration was employed to simplify the system and facilitate the visualization of electrode performance of the liquid side especially. Figure 2a shows the variation of RHVFC energy density with the applied current density during discharge cycles. At all current densities tested the N-G/SGL results in higher energy densities than rGO/SGL and pristine SGL. These results are comparable to a standard VRFB with enhanced capacity (using 3 M vanadium compared to 0.8 M in our work, especially by ignoring the volume of H_2 gas generated during the charging of the RHVFC).[28] Considering the fact that the kinetics of the VO_2^+/VO^{2+} couple is slower than the H^+/H_2 half-cell in the RHVFC, this performance improvement is attributable to a combined action of enhanced ECSA (as supported by BET results in Figure 1f) and improved catalytic activity of N-G/SGL electrodes.[27] The rGO/SGL electrodes show a marginal improvement (around 5% at higher current densities as seen in Figure 2a) in the electrochemical performance of the VO_2^+/VO^{2+} redox couple compared to pristine CP (SGL) which exhibits the lowest energy density of 21 Wh L^{-1} (Figure 2a) because of a low ECSA combined with poor wettability and low corrosion resistance.[2] The result obtained for N-G/SGL electrodes is also similar to the observation made by Jin et al.,[18] highlighting the role of catalytic activity and fast electron transfer in redox reactions involving VO_2^+/VO^{2+}, enabled by N-G modification of the carbon electrodes.

The energy efficiency of electrodes at four different current densities is shown in Figure 2b. Coulombic and voltaic efficiencies used to determine these values are reported in the Supporting Information. In particular, when current density is increased, a larger mass flow of active species to the electrode surface comes at the cost of depleting the reactants. Consequently, a higher mass transport overpotential is caused, which reduces the charging/discharging capacity, resulting in a decline in the efficiencies.[29] N-G-modified SGL outperformed both rGO/SGL and pristine SGL, which is in line with Figure 2a. The fact that we obtained an energy efficiency of slightly above 60% at a high current density of 200 mA cm^{-2} (Figure 2b) is again reflective of larger ECSA of N-G/SGL which lowers mass transport overpotential for the RHVFC. These results are consistent with a practical VRFB operating at similar or higher current densities of 100 mA cm^{-2} by using thermally treated N-doped PAN-based graphite felts.[30] The variation of the RHVFC cell voltage against specific cell capacity is shown in Figure 2c, where N-G electrodes outperform both rGO and the pristine SGL electrodes. Furthermore, these experiments were performed at a relatively lower current density of 50 mA cm^{-2} to reduce the effects of side reactions as far as possible.

A higher peak power density close to 410 mW cm^{-2} was obtained with N-G SGL as shown in Figure 2d in comparison to that for the pristine SGL, which achieved a value of 293 mW cm^{-2} (this was in fact much higher than the original value of 114 mW cm^{-2} using the same SGL (CP) as reported by Yufit and co-workers).[31] However, these peak power densities are lower than those reported[19] because this HRFC design, similar to that reported earlier,[12] was not optimized in terms of using a more appropriate combination of the membrane electrode assembly, compression, and flow channel configuration. In addition, our RHVFC was not a single-pass system due to which the resultant peak power densities were about an order of magnitude lower than a recently optimized VRFB.[16] The same also applies when our N-G-modified SGL is compared with a free-standing carbon electrode (derived from carbonizing cocoons) having enriched nitrogen defects and oxygen functional groups yielding ∼20% increase in energy efficiency of RFBs as reported recently.[32]

Figure 2e shows the cycling performance of the RHVFC. The overall energy efficiencies obtained by using N-G-modified electrodes were about 75% for N-G-modified SGL even after 150 cycles (by which time the cells reached steady-state conditions) at a high current density of 100 mA cm^{-2}. It should also be noted that cycling for long periods can result in performance decay, which are not always necessarily due to electrode degradation due to reasons including water evaporation and electrolyte viscosity (lower VE) and/or redox couple crossover via the membrane to the gaseous half-cell. This cycling performance compares well with the main figures of merit of standard VRFBs as displayed in Table S2, which highlights the realistic potential of RHVFC technology when employing N-G-modified carbonaceous electrodes for practical applications. Figure 2f provides the discharge capacity utilization of the RHVFC upon cycling, where fluctuations observed throughout the testing are most likely due to nonoptimized compression of the electrodes (indicating that further improvements are possible with

https://dx.doi.org/10.1021/acsami.0c17616
ACS Appl. Mater. Interfaces 2020, 12, 53869−53878

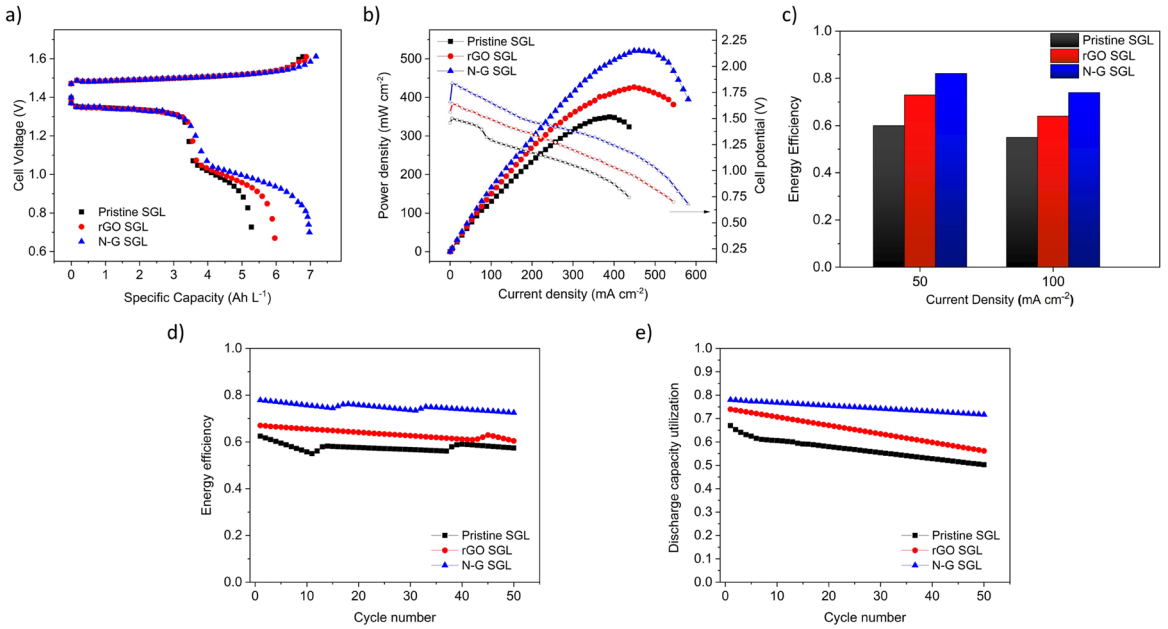

Figure 3. Electrochemical performance of RHMnFC using pristine CP (SGL), rGO/CP, and N-G/CP: (a) Fifth charge and discharge capacity. Electrolyte was 1 M $MnCO_3$ dissolved with 1 M $Ti(SO_4)_2$ in 3 M H_2SO_4 at a flow rate of 50 mL min^{-1} in a 5 cm^2 active reactor. Hydrogen flow rate was 30 mL min^{-1}. A constant charge/discharge current density of 100 mA cm^{-2} was used for all experiments. (b) Polarization and power density curves using the same electrolytic conditions but at a raised hydrogen flow rate of 100 mL min^{-1}. (c) Energy efficiencies as a function of two operating current densities. (d) Energy efficiency variation as a function of cycle number operating at 100 mA cm^{-2} under same electrolytic conditions and gaseous flow rate of 30 mL min^{-1}. (e) Discharge capacity utilization for 50 cycles also operating at 100 mA cm^{-2}.

porosity control and electrolyte accessibility, as shown in a recent work on VRFBs).[16] The electrolyte utilization is another important factor, which in the case of N-G/SGL is improved on average by 20% in comparison to the performance of pristine SGL as a consequence of low overpotential and reduced ohmic losses due to better wetting of the CP as well as higher ECSA for the VO_2^+/VO^{2+} redox couple.[27,30] Similar trends of performance enhancements have also been recently reported on phosphorus-doped carbon electrodes in terms of cycling performance at high current densities in the VRFB.[33]

We have also performed postcycling analysis of these electrodes via SEM, XPS, and Raman which shows that the morphology of graphene deposited SGL was largely retained (see Figures S1−S12). This indicates a remarkable stability of these electrodes as electrochemical reactions attained steady-state conditions, while catalytically active, which corroborates with the observed electrochemical performance (Figure 2). In addition, increasing BET surface areas due to cycling (see Table S3) may imply an increased presence of oxygenated functional groups at the graphene edges that contribute to their wetting properties. Additionally, the graphitic structure of N-G inhibits degradation while maintaining a good electrode conductivity.[27]

The next HRFC that has high commercial potential is the RHMnFC because of the use of low-cost electrolyte (manganese is more abundant compared with vanadium) and higher operating cell voltage, which leads to decreased stack costs. In addition, Mn is not volatile at room temperature (as Br from the positive side of the RHBrFC is toxic in the vapor phase),[10] resulting in inherently safer systems. Figure 3a shows the charge and discharge performance of an RHMnFC using N-G/SGL-modified electrodes at a practical operating current density of 100 mA cm^{-2}, where N-G clearly outperformed rGO-SGL and pristine SGL electrodes. We note that this is the first report of N-G-doped carbon electrode being exploited in the RHMnFC, which therefore can incentivize fundamental studies on the interaction of Mn and Ti (titanium is typically added to electrolytes to suppress the formation of MnO_2 that causes capacity fade)[20] on both graphene and CNTs for optimization of HRFCs.

Two different discharge voltage plateaus are observed during discharge for instance around 1.1 and 1.3 V at 100 mA cm^{-2} (Figure 3a). A similar phenomenon was also reported in an earlier work.[20] This is attributable to a high initial overpotential which gradually decreases with discharge and reaches a constant voltage value after ∼3 Ah L^{-1}. This may be due to the transport of Mn and Ti species back to the liquid reservoir by electroosmotic drag, thus removing adsorbed metal ions from the catalyst surface (hydrogen side) and progressively facilitating the access of H_2 to the more reactive Pt sites. Additionally, the depletion of active species at the liquid side leads to mass transport limitations which, in conjunction with the stable potential at the negative electrode, can promote a cell voltage transition toward a lower discharge plateau as reported previously.[20]

Figure 3b shows the polarization and power density curves of the RHMnFC. Without performing *IR* correction, we achieved a peak power density of 521 mW cm^{-2} with the N-G-modified SGL, which is very close to untreated graphite felt electrodes used in hybrid manganese flow cells.[20] This therefore indicates that further improvements are possible by optimizing the membrane electrode assembly, flow distribution channels, electrolyte management, and electrode compression. Figure 3c shows the energy efficiencies of the system at two operating current densities for practical consideration for scaling up. At 100 mA cm^{-2}, the efficiency of N-G-modified CP in the RHMnFC of 75% is comparable to that reported for a similar system using standard graphite felt electrodes.[20] It is

https://dx.doi.org/10.1021/acsami.0c17616
ACS Appl. Mater. Interfaces 2020, 12, 53869−53878

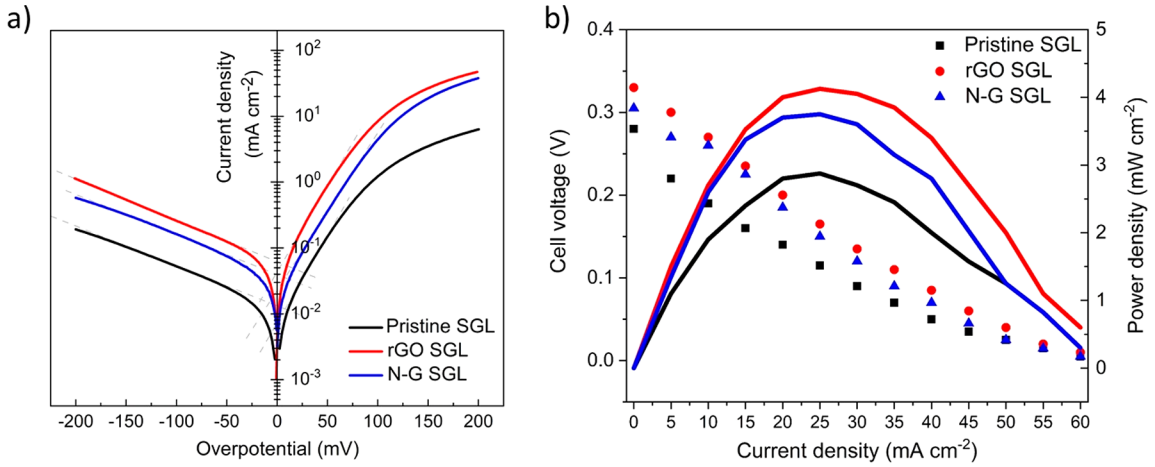

Figure 4. (a) S-Air cell Tafel plots of pristine CP (or SGL), rGO/CP, and N-G/CP in 1 M Na_2S_2/1 M NaOH versus an Ag/AgCl reference in a three-electrode cell. (b) Polarization and power density curves of the full S-Air RFC.

also comparable to efficiencies reported on some VRFB studies as shown in Table S2.

Figure 3d shows the energy efficiencies of RHMnFC for 50 cycles at a current density of 100 mA cm^{-2}. It is observed that the average energy efficiency for N-G/SGL of 75% is comparable to that for graphite felt electrodes reported in a previous study.[20] Figure 3e shows the discharge capacity utilization, which is about 33% higher on average for N-G/SGL in comparison to pristine SGL. Additionally, a slow decline in the trend is observed especially for rGO/SGL and pristine SGL. For N-G/SGL, the decline is gradual but in a stable manner and indicating a possibility that the onset of electrode surface corrosion increases the ECSA and leads to similar performance when using felts.[20] Nevertheless, these findings point out that employing N-G-modified felts can be beneficial to HRFC performance, similar to what has been reported on organic redox flow batteries.[34]

Lastly, we have tested the suitability of these electrodes in S-Air HRFC (in a three-electrode system), which is also for the first time with this type of electrode. We here aimed at improving kinetics of the polysulfide chemistry rather than performing a full S-Air cell (as both RHVFC and RHMnFC were studied as full cells) by evaluating solely the potential benefits that N-G/SGL or rGO/SGL electrodes can bring to polysulfide chemistry (without considering potential losses due to the high overpotential of ORR/OER).[35] Figure 4a shows the electrochemical behavior of pristine SGL, rGO/SGL, and N-G/SGL when tested in a 1 M sodium polysulfide alkaline solution in a three-electrode reactor. The Tafel plots qualitatively show that rGO/SGL results in a higher exchange current density for polysulfide reactions in comparison to N-G (as shown in Table S4). This outcome is different from those that were obtained for an RHVFC under acidic conditions, and it appears that rGO/SGL is a better catalyst for polysulfide reactions than N-G/SGL. Looking at the amorphous nature of rGO when deposited on SGL (from Raman data in Figure 1g), the alkaline-based polysulfide reactions appear to be benefited more from catalytic sites for charge transfer, which is apparently less probable with N-G/SGL because the interaction of OH^- or polysulfide anions with oxygenated functional groups is more favorable than nitrogenous species.[36] This implies that the oxygen-based functional groups present in rGO are more favorable for polysulfide reactions. However, N-G/SGL does provide better electrochemical activity than pristine SGL as shown in Figure 4a.

Figure 4b demonstrates the polarization tests of the 5 cm^2 single-cell S-Air RFC. A maximum power density of ~3.7 mW cm^{-2} was achieved at the current density of 27.5 mA cm^{-2} for N-G SGL, which was just less than twice of the maximum power density achieved with an untreated SGL 10AA carbon paper (2.8 mW cm^{-2}) anode. Additionally, the peak power density of rGO SGL is about 4.2 mW cm^{-2}, which is consistent with the result shown in the Tafel plot (Figure 4a).

Finally, we have performed a cost analysis for rationalizing the selection and scaling up of these HRFCs (the cost of vanadium is taken from the Roskill market report Web page[37]), and more details are in the Supporting Information. As in flow battery systems, since the power and energy are fully decoupled, the knowledge of the cost can aid in tailoring HRFCs depending on their application. For example, for applications requiring days or weeks of electricity storage, the cost analysis indicates that S-Air flow systems will be most suitable, while for shorter duration of storage (4−10 h) RHMnFCs will be more appropriate.

In general, even though the cost of VRFB and RHVFC (Figure 5) appears similar at the same continuous discharge power density, RHVFC becomes cheaper with increased hours of storage, which is due to less vanadium used in the system. The RHVFC cost can be further reduced in comparison to VRFB if HRFC systems operate at higher power densities. This is relatively straightforward to achieve because the limitation here is only from the vanadium positive electrode since the

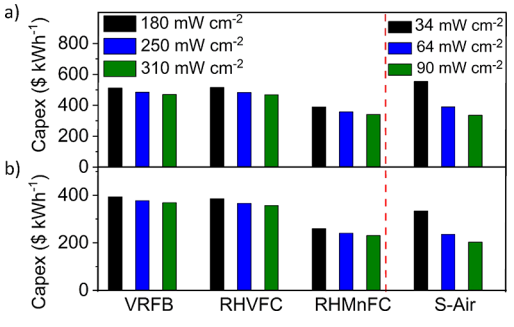

Figure 5. System cost comparison between various flow batteries (a) for 6 h of storage and (b) for 10 h of storage.

https://dx.doi.org/10.1021/acsami.0c17616
ACS Appl. Mater. Interfaces 2020, 12, 53869−53878

hydrogen redox reaction is facile and much faster than V(II)/V(III) in VRFBs.[31]

Once optimized, the cost of the RHMnFC system is significantly lower than both VRFB and RHVFC, and this is solely due to the use of a much cheaper Mn-based electrolyte. The cost of the S-Air system is high for shorter durations of storage. This is mainly due to a lower power density of the system, limited by the reactions on air electrodes. As the main contributors to the cost here are cell stacks and balance of plant, the system cost reduces significantly with increased storage duration, especially when going beyond 10 h (into days and weeks). With such a long duration the cost of the system will be mostly defined by the cost of the electrolyte (concentrated polysulfides dissolved in aqueous hydroxide solution), which is much cheaper than the low-cost manganese-based electrolytes.[3]

4. CONCLUSION

We have investigated three types of hybrid redox flow cell (HRFC) systems by using hybrid electrodes consisting of electrophoretically deposited nitrogen-doped graphene on carbon paper. We have demonstrated that these electrodes are capable of meeting the harsh electrochemical requirements for these HRFCs, evidenced by their enhanced performance and operability, attributed to the high specificity of these electrodes coming from the synergistic effects of enhanced electrochemical surface area, chemical/electrochemical stability, and catalytic activity. Furthermore, the estimated system cost shows that HRFCs are potentially low-cost alternatives to the commercial standard VRFB. The studies reported herein can provide new incentives for further optimization of HRFCs involving the replacement of conventional carbon electrodes with N-G-modified electrodes or free-standing hierarchical nanomaterial structures to extend their range and scope of the operating conditions.

■ ASSOCIATED CONTENT

Supporting Information

The Supporting Information is available free of charge at https://pubs.acs.org/doi/10.1021/acsami.0c17616.

> Some historical developments of RFCs, use of N-G for VRFBs, electrochemical performances (such as impedance for RHVFC), XPS, TEM, and other morphological characterizations; additional cycling data of the RHVFC and RHMnFC (e.g., Coulombic and voltaic efficiencies); justification for costing these hybrid systems (PDF)

■ AUTHOR INFORMATION

Corresponding Authors

Barun Kumar Chakrabarti − *WMG, Warwick Electrochemical Engineering Group, Energy Innovation Centre, University of Warwick, Coventry CV4 7AL, United Kingdom; RFC Power Ltd., London SW7 2PG, United Kingdom;* orcid.org/0000-0002-0172-986X; Email: barun.chakrabarti@warwick.ac.uk

J. Rubio-Garcia − *Department of Chemistry, Imperial College London, London SW7 2AZ, United Kingdom;* Email: j.rubio-garcia@imperial.ac.uk, j.rubio.garc@gmail.com

Authors

Jingyu Feng − *Department of Chemical Engineering, Imperial College London, London SW7 2AZ, United Kingdom*

Evangelos Kalamaras − *WMG, Warwick Electrochemical Engineering Group, Energy Innovation Centre, University of Warwick, Coventry CV4 7AL, United Kingdom;* orcid.org/0000-0002-8234-4274

Chandramohan George − *Dyson School of Design Engineering, Imperial College London, London SW7 2AZ, United Kingdom;* orcid.org/0000-0003-2906-6399

Hui Luo − *Department of Chemical Engineering, Imperial College London, London SW7 2AZ, United Kingdom*

Yuhua Xia − *Department of Earth Science and Engineering, Imperial College London, London SW7 2AZ, United Kingdom*

Vladimir Yufit − *Addionics Ltd., London W12 0BZ, United Kingdom*

Maria-Magdalena Titirici − *Department of Chemical Engineering, Imperial College London, London SW7 2AZ, United Kingdom;* orcid.org/0000-0003-0773-2100

Chee Tong John Low − *WMG, Warwick Electrochemical Engineering Group, Energy Innovation Centre, University of Warwick, Coventry CV4 7AL, United Kingdom;* orcid.org/0000-0003-4411-9890

Anthony Kucernak − *RFC Power Ltd., London SW7 2PG, United Kingdom; Department of Chemistry, Imperial College London, London SW7 2AZ, United Kingdom*

Nigel P. Brandon − *RFC Power Ltd., London SW7 2PG, United Kingdom; Department of Earth Science and Engineering, Imperial College London, London SW7 2AZ, United Kingdom*

Complete contact information is available at: https://pubs.acs.org/10.1021/acsami.0c17616

Notes

The authors declare no competing financial interest.

Supporting data are available on request: please contact the corresponding authors on barunkumar77uk@gmail.com.

■ ACKNOWLEDGMENTS

This work has received financial support from EPSRC ISCF Wave 1 : 3D electrodes from 2D materials (EP/R023034/1) and Innovate UK's HYPAREST awarded to RFC Power and Imperial College (133462). Dan Nir, currently Commercial Head of Funding Circle Netherlands and ex-student from T. U. Delft, is acknowledged for helping with the horizontal EPD reactor design. C.G. acknowledges funding from The Royal Society, London, for an URF (UF160573) and C.T.J.L. is grateful to Shanghai Jiao Tong University - Warwick Joint Seed Fund for financial support. Authors gratefully acknowledge UKRI for facilitating full open access of this article via the Creative Commons Attribution (CC-BY) license.

■ REFERENCES

(1) Brushett, F. R.; Aziz, M. J.; Rodby, K. E. On Lifetime and Cost of Redox-Active Organics for Aqueous Flow Batteries. *ACS Energy Lett.* **2020**, *5* (3), 879−884.

(2) Gencten, M.; Sahin, Y. A critical review on progress of the electrode materials of vanadium redox flow battery. *Int. J. Energy Res.* **2020**, *44*, 7903−7923.

(3) Li, Z.; Pan, M. S.; Su, L.; Tsai, P.-C.; Badel, A. F.; Valle, J. M.; Eiler, S. L.; Xiang, K.; Brushett, F. R.; Chiang, Y.-M. Air-Breathing

Aqueous Sulfur Flow Battery for Ultralow-Cost Long-Duration Electrical Storage. *Joule* **2017**, *1* (2), 306−327.
(4) Viswanathan, V.; Crawford, A.; Stephenson, D.; Kim, S.; Wang, W.; Li, B.; Coffey, G.; Thomsen, E.; Graff, G.; Balducci, P.; Kintner-Meyer, M.; Sprenkle, V. Cost and performance model for redox flow batteries. *J. Power Sources* **2014**, *247*, 1040−1051.
(5) Zhou, H.; Zhang, H.; Zhao, P.; Yi, B. A comparative study of carbon felt and activated carbon based electrodes for sodium polysulfide/bromine redox flow battery. *Electrochim. Acta* **2006**, *51* (28), 6304−6312.
(6) Lai, Y. Y.; Li, X.; Liu, K.; Tung, W.-Y.; Cheng, C.-F.; Zhu, Y. Stable Low-Cost Organic Dye Anolyte for Aqueous Organic Redox Flow Battery. *ACS Appl. Energy Mater.* **2020**, *3* (3), 2290−2295.
(7) Cheng, Y.; Wang, X.; Huang, S.; Samarakoon, W.; Xi, S.; Ji, Y.; Zhang, H.; Zhang, F.; Du, Y.; Feng, Z.; Adams, S.; Wang, Q. Redox Targeting-Based Vanadium Redox-Flow Battery. *ACS Energy Lett.* **2019**, *4* (12), 3028−3035.
(8) Lin, G.; Chong, P. Y.; Yarlagadda, V.; Nguyen, T. V.; Wycisk, R. J.; Pintauro, P. N.; Bates, M.; Mukerjee, S.; Tucker, M. C.; Weber, A. Z. Advanced Hydrogen-Bromine Flow Batteries with Improved Efficiency, Durability and Cost. *J. Electrochem. Soc.* **2016**, *163* (1), A5049−A5056.
(9) Rubio-Garcia, J.; Kucernak, A.; Parra-Puerto, A.; Liu, R.; Chakrabarti, B. Hydrogen/functionalized benzoquinone for a high-performance regenerative fuel cell as a potential large-scale energy storage platform. *J. Mater. Chem. A* **2020**, *8*, 3933−3941.
(10) Cho, K. T.; Tucker, M. C.; Ding, M.; Ridgway, P.; Battaglia, V. S.; Srinivasan, V.; Weber, A. Z. Cyclic Performance Analysis of Hydrogen/Bromine Flow Batteries for Grid-Scale Energy Storage. *ChemPlusChem.* **2015**, *80* (2), 402−411.
(11) Zheng, Q.; Xing, F.; Li, X.; Liu, T.; Lai, Q.; Ning, G.; Zhang, H. Investigation on the performance evaluation method of flow batteries. *J. Power Sources* **2014**, *266*, 145−149.
(12) Chakrabarti, B.; Yufit, V.; Kavei, A.; Xia, Y.; Stevenson, G.; Kalamaras, E.; Luo, H.; Feng, J.; Tariq, F.; Taiwo, O.; Titirici, M.-M.; Brandon, N. Charge/discharge and cycling performance of flexible carbon paper electrodes in a regenerative hydrogen/vanadium fuel cell. *Int. J. Hydrogen Energy* **2019**, *44* (57), 30093−30107.
(13) Zhang, D.; Forner-Cuenca, A.; Taiwo, O. O.; Yufit, V.; Brushett, F. R.; Brandon, N. P.; Gu, S.; Cai, Q. Understanding the role of the porous electrode microstructure in redox flow battery performance using an experimentally validated 3D pore-scale lattice Boltzmann model. *J. Power Sources* **2020**, *447*, 227249.
(14) Jervis, R.; Kok, M. D. R.; Neville, T. P.; Meyer, Q.; Brown, L. D.; Iacoviello, F.; Gostick, J. T.; Brett, D. J. L.; Shearing, P. R. In situ compression and X-ray computed tomography of flow battery electrodes. *J. Energy Chem.* **2018**, *27* (5), 1353−1361.
(15) Chakrabarti, B.; Rubio-Garcia, J.; Kalamaras, E.; Yufit, V.; Tariq, F.; Low, C. T. J.; Kucernak, A.; Brandon, N. Evaluation of a Non-Aqueous Vanadium Redox Flow Battery Using a Deep Eutectic Solvent and Graphene-Modified Carbon Electrodes via Electrophoretic Deposition. *Batteries* **2020**, *6* (3), 38.
(16) Jiang, H. R.; Sun, J.; Wei, L.; Wu, M. C.; Shyy, W.; Zhao, T. S. A high power density and long cycle life vanadium redox flow battery. *Energy Stor. Mater.* **2020**, *24*, 529−540.
(17) Greco, K. V.; Forner-Cuenca, A.; Mularczyk, A.; Eller, J.; Brushett, F. R. Elucidating the Nuanced Effects of Thermal Pretreatment on Carbon Paper Electrodes for Vanadium Redox Flow Batteries. *ACS Appl. Mater. Interfaces* **2018**, *10* (51), 44430−44442.
(18) Jin, J.; Fu, X.; Liu, Q.; Liu, Y.; Wei, Z.; Niu, K.; Zhang, J. Identifying the Active Site in Nitrogen-Doped Graphene for the VO2+/VO2+ Redox Reaction. *ACS Nano* **2013**, *7* (6), 4764−4773.
(19) Tenny, K. M.; Lakhanpal, V. S.; Dowd, R. P.; Yarlagadda, V.; Van Nguyen, T. Impact of Multi-Walled Carbon Nanotube Fabrication on Carbon Cloth Electrodes for Hydrogen-Vanadium Reversible Fuel Cells. *J. Electrochem. Soc.* **2017**, *164* (12), A2534−A2538.
(20) Rubio-Garcia, J.; Kucernak, A.; Zhao, D.; Li, D.; Fahy, K.; Yufit, V.; Brandon, N.; Gomez-Gonzalez, M. Hydrogen/manganese hybrid redox flow battery. *J. Phys. Energy* **2019**, *1* (1), 015006.
(21) Forner-Cuenca, A.; Penn, E. E.; Oliveira, A. M.; Brushett, F. R. Exploring the Role of Electrode Microstructure on the Performance of Non-Aqueous Redox Flow Batteries. *J. Electrochem. Soc.* **2019**, *166* (10), A2230−A2241.
(22) Brandon, N.; Kucernak, A.; Yufit, V. Regenerative fuel cells. US patent US2013/0330644A1, 2013.
(23) Chai, G.-L.; Qiu, K.; Qiao, M.; Titirici, M.-M.; Shang, C.; Guo, Z. Active sites engineering leads to exceptional ORR and OER bifunctionality in P,N Co-doped graphene frameworks. *Energy Environ. Sci.* **2017**, *10* (5), 1186−1195.
(24) Tariq, F.; Rubio-Garcia, J.; Yufit, V.; Bertei, A.; Chakrabarti, B. K.; Kucernak, A.; Brandon, N. Uncovering the mechanisms of electrolyte permeation in porous electrodes for redox flow batteries through real time in situ 3D imaging. *Sustain. Energy Fuels* **2018**, *2* (9), 2068−2080.
(25) Chakrabarti, B.; Nir, D.; Yufit, V.; Tariq, F.; Rubio-Garcia, J.; Maher, R.; Kucernak, A.; Aravind, P. V.; Brandon, N. Performance Enhancement of Reduced Graphene Oxide-Modified Carbon Electrodes for Vanadium Redox-Flow Systems. *ChemElectroChem.* **2017**, *4* (1), 194−200.
(26) Pino-Muñoz, C. A.; Chakrabarti, B. K.; Yufit, V.; Brandon, N. P. Characterization of a Regenerative Hydrogen-Vanadium Fuel Cell Using an Experimentally Validated Unit Cell Model. *J. Electrochem. Soc.* **2019**, *166* (15), A3511−A3524.
(27) Yang, D.-S.; Lee, J. Y.; Jo, S.-W.; Yoon, S. J.; Kim, T.-H.; Hong, Y. T. Electrocatalytic activity of nitrogen-doped CNT graphite felt hybrid for all-vanadium redox flow batteries. *Int. J. Hydrogen Energy* **2018**, *43* (3), 1516−1522.
(28) Roe, S.; Menictas, C.; Skyllas-Kazacos, M. A High Energy Density Vanadium Redox Flow Battery with 3 M Vanadium Electrolyte. *J. Electrochem. Soc.* **2016**, *163* (1), A5023−A5028.
(29) Pezeshki, A. M.; Sacci, R. L.; Veith, G. M.; Zawodzinski, T. A.; Mench, M. M. The Cell-in-Series Method: A Technique for Accelerated Electrode Degradation in Redox Flow Batteries. *J. Electrochem. Soc.* **2016**, *163* (1), A5202−A5210.
(30) Yoon, S. J.; Kim, S.; Kim, D. K.; Yu, D. M.; Hempelmann, R.; Hong, Y. T.; So, S. Nitrogen-Doping Through Two-Step Pyrolysis of Polyacrylonitrile on Graphite Felts for Vanadium Redox Flow Batteries. *Energy Fuels* **2020**, *34* (4), 5052−5059.
(31) Yufit, V.; Hale, B.; Matian, M.; Mazur, P.; Brandon, N. P. Development of a Regenerative Hydrogen-Vanadium Fuel Cell for Energy Storage Applications. *J. Electrochem. Soc.* **2013**, *160* (6), A856−A861.
(32) Wang, R.; Li, Y. Twin-cocoon-derived self-standing nitrogen-oxygen-rich monolithic carbon material as the cost-effective electrode for redox flow batteries. *J. Power Sources* **2019**, *421*, 139−146.
(33) Wang, R.; Li, Y.; Wang, Y.; Fang, Z. Phosphorus-doped graphite felt allowing stabilized electrochemical interface and hierarchical pore structure for redox flow battery. *Appl. Energy* **2020**, *261*, 114369.
(34) Cao, J.; Zhu, Z.; Xu, J.; Tao, M.; Chen, Z. Nitrogen-doped porous graphene as a highly efficient cathodic electrocatalyst for aqueous organic redox flow battery application. *J. Mater. Chem. A* **2017**, *5* (17), 7944−7951.
(35) grosse Austing, J.; Nunes Kirchner, C.; Komsiyska, L.; Wittstock, G. Investigation of crossover processes in a unitized bidirectional vanadium/air redox flow battery. *J. Power Sources* **2016**, *306*, 692−701.
(36) Li, G.; Wang, X.; Seo, M. H.; Li, M.; Ma, L.; Yuan, Y.; Wu, T.; Yu, A.; Wang, S.; Lu, J.; Chen, Z. Chemisorption of polysulfides through redox reactions with organic molecules for lithium−sulfur batteries. *Nat. Commun.* **2018**, *9* (1), 705.
(37) https://roskill.com/market-report/vanadium/.

https://dx.doi.org/10.1021/acsami.0c17616
ACS Appl. Mater. Interfaces 2020, 12, 53869−53878